

Mediterranean waters along and across the Strait of Gibraltar, characterization and zonal modification.

Cristina Naranjo⁽¹⁾, Simone Sammartino⁽¹⁾, Jesús García-Lafuente⁽¹⁾,
María J. Bellanco⁽²⁾, Isabelle Taupier-Letage⁽³⁾.

⁽¹⁾ Grupo de Oceanografía Física, Universidad de Málaga, 29071 Málaga, Spain

⁽²⁾ Centro Oceanográfico de Cádiz, Instituto Español de Oceanografía (IEO), 11006 Cádiz, Spain.

⁽³⁾ Aix Marseille Université, CNRS, Université de Toulon, IRD, MIO UM 110, Antenne de la Seyne, 83507 La Seyne, France

Abstract

Hydrological data collected in the Strait of Gibraltar have been used to examine the distribution and spatial-temporal evolution of the water masses in the area. The spatial variability has been addressed by means of a clustering method that determines the affinity of a collection of Temperature-Salinity samples to one of the water masses involved in the exchange. The method, which has been applied to a nearly-synoptic data set, highlights the clear evolution of the Mediterranean Waters as they flow westward through the Strait. While up to four different Mediterranean Waters are spatially distinguishable east of the main sill of Camarinal in the Strait, most of their differentiating characteristics are eroded after flowing over this restrictive topography due to mixing. West of the sill, therefore, speaking of a unique Mediterranean Water seems more appropriate. The opposite applies to the North Atlantic Central Water, which is noticeably modified along its path to the Mediterranean Sea, most of its transformation taking place in the Camarinal sill surroundings. A series of repeated transects carried out in the eastern and western margins of the Strait, provided a temporal analysis of the water masses evolution: the temporal variability manifests seasonality in the surface waters, while interannual signal is exclusively detected in the deeper water masses. It is worth remarking the statistically significant positive trend of Western Mediterranean Deep Water ($0.009^{\circ}\text{C}/\text{year}$) and Winter Intermediate Water ($0.03^{\circ}\text{C}/\text{year}$), with the latter showing also intermittent occurrence in the Strait.

Keywords:

Strait of Gibraltar, Mediterranean outflow, water masses, cluster analysis.

1. Introduction

In the Mediterranean Sea (MedS, hereinafter) the Atlantic Water (AW) that flows in through the Strait of Gibraltar (SoG) is modified by evaporation and transformed into Mediterranean water, saltier and denser, which ends up flowing out through the SoG to the Atlantic Ocean. A simplified Mediterranean basin is schematized by an eastern and a western basins connected by the Strait of Sicily. In the eastern basin, Levantine Intermediate Water (LIW) is formed through open-sea convection. In the western basin, more specifically in the Gulf of Lion, Western Mediterranean Deep Water (WMDW) is formed by deep convection. It was known since long ago that the LIW was a permanent contributor to the outflow. However, the possibility that the WMDW was participating significantly in the outflow was first presented by Stommel et al. (1973), who attributed its presence to the Bernoulli aspiration of this water from great depth in the MedS over the main sill of Camarinal in the SoG. Subsequently, other authors have revisited the topic and stressed this thought (Bryden et al., 1982; Whitehead, 1985; Gascard & Richez, 1985; Kinder & Parrilla, 1987; Kinder & Bryden, 1990; García-Lafuente, et al., 2007; Naranjo et al., 2012, 2014). At present, it is accepted that this deep water is a permanent part of the outflow.

Studies dealing with the outflow within and nearby the SoG used to focus on the two main MWs, the LIW and the WMDW (Bray, et al., 1995; Pettigrew, 1989; García-Lafuente, et al., 2007), which are easily identified by the maximum and minimum potential temperature, respectively, in the densest part of the θ -S diagram (Gascard & Richez, 1985). Recent efforts made to clarify the hydrological characteristics of the water masses leaving the MedS through the SoG have suggested the presence of other Mediterranean water masses, more specifically, the Tyrrhenian Dense Water (TDW) and the Winter Intermediate Water (WIW) (Millot et al., 2006; Millot, 2009, 2013, 2014; Rhein et al., 1999). The first is formed by the mixing of old WMDW residing in the Tyrrhenian Sea with newly entered LIW flowing into the western MedS through the Strait of Sicily (Rhein et al., 1999; Millot et al., 2006). The WIW is formed by convection of cooled Modified Atlantic Water under severe winter condition along the continental shelf of the Liguro-Provençal sub-basin and Catalan Sea (Conan & Millod, 1995; Vargas-Yáñez, et al., 2012). At its source, it is the coolest water in the Western MedS (Salat & Font, 1987; Millot, 1999; Lopez-Jurado et al., 1995) and it is easily

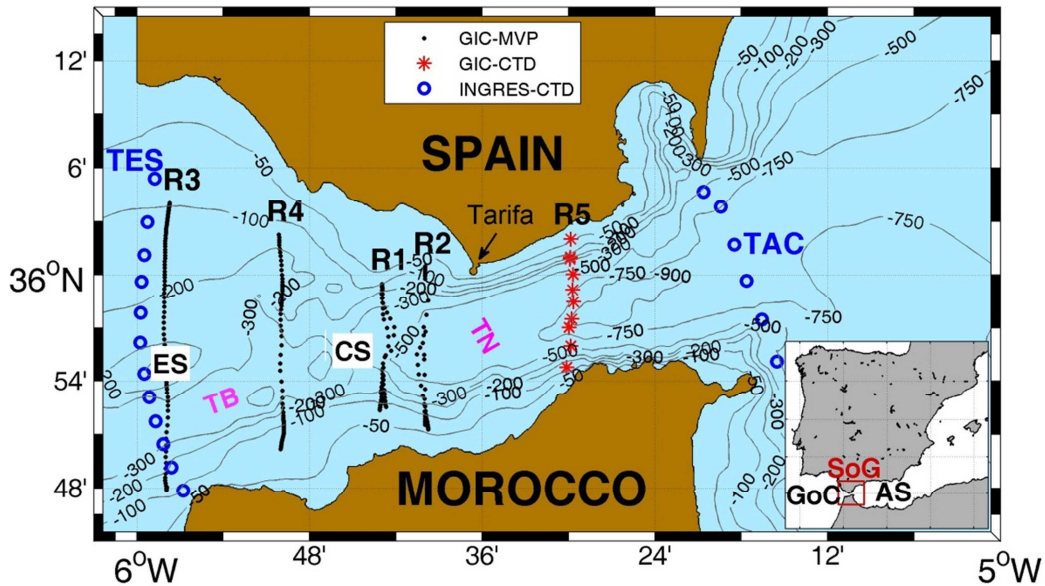
38 detected in any θ -S diagram by a minimum of potential temperature
39 between $\sigma_\theta=28.0$ and $\sigma_\theta=29.0$ (Millot, 2014).

40 With the aim of contributing to the last findings and to offer a clear and
41 standardized method to classify the water masses in the SoG, this work
42 proposes a statistical method to automatically classify every water mass
43 involved in the exchange. Two sets of data, described in Section 2, were
44 specifically collected in the SoG area to address the topic. The first dataset
45 was acquired during the Gibraltar International Campaign (GIC, Section
46 2.1) and the second one throughout the lifespan of the INGRES projects
47 (Section 2.2) funded by the Spanish Government. Section 3 describes the
48 data processing, paying special attention to the description of the proposed
49 method of analysis (Section 3.2). The hydrological information contained in
50 these two sets of data has been exploited in different ways in this study.
51 GIC data were collected during a very short period and allow us for making
52 a quasi-synoptic description of the water masses distribution in the SoG. On
53 the contrary, INGRES data gather samples spanning a rather long period of
54 time and have the potential of addressing the time variability and evolution
55 of the water masses. Section 4 discusses both topics in Subsections 4.1
56 (GIC) and 4.2 (INGRES) respectively. Finally, Section 5 summarizes the
57 findings and conclusions of the study.

58 2. Data

59 2.1. CTD and MVP data from Gibraltar International Campaign

60 In the framework of the international Hydrochanges programme sponsored
61 by the Commission Internationale pour l'Exploration Scientifique de la
62 Méditerranée (Mediterranean Science Commission, CIESM), the French
63 *Mediterranean Institute of Oceanography* carried out the *Gibraltar*
64 *International Campaign* on board the R/V Tethys II from the 4th to the 6th
65 July 2012. The cruise was aimed at obtaining high resolution Conductivity-
66 Temperature-Depth (CTD) profiles along the transects showed in Figure 1 in
67 order to give an accurate water mass characterization and distribution of
68 Mediterranean waters within the SoG. Except for section R5, a Moving
69 Vessel Profiler (MVP) was employed; this instrument allows semi-
70 autonomous sampling of the water column with very high spatial resolution.
71 A drawback of the MVP mounted on the Tethys's deck was its limited range
72 depth. Transect R5 and a repetition of transect R2 were sampled with a CTD
73 probe that reached the seafloor. The CTD vertical profiles in these transects,
74 however, are substantially further apart than MVP profiles.



75

76 Figure 1. Map of the Strait of Gibraltar showing bathymetric contours, in meters. The black
 77 dots and red asterisks indicate the location of the vertical profiles along the 5 sampled
 78 sections for MVP and CTD data in GIC campaign (R1-R5), respectively. Blue circles represent
 79 the two CTD sections regularly repeated in the INGRES project (TAC and TES). The main sills
 80 of Espartel (ES) and Camarinal (CS), the small Tangier Basin (TB) between them and the
 81 Tarifa Narrows (TN) are also indicated. The inset shows the location of the Strait (SoG)
 82 between the Alboran Sea (AS), the westernmost basin of the Mediterranean Sea, and the
 83 Gulf of Cadiz (GoC) in the Atlantic Ocean.

84 2.2. Historical CTD data from INGRES project

85 The INGRES projects were initiated in year 2004 with the objective of
 86 monitoring the Mediterranean outflow and its variability in response to
 87 subinertial and longer-term forcing as well as the hydrological properties of
 88 the densest and, hence, deepest Mediterranean water leaving the MedS. At
 89 the time of this writing the monitoring, which is planned to be kept on
 90 position *sine die*, is still in progress. Whenever the station was serviced
 91 (every 4 or 6 months) and weather permitting, CTD transects were
 92 accomplished. Among them, transects labeled TES and TAC in Figure 1 have
 93 been repeatedly sampled during the lifespan of INGRES projects. They
 94 make up an unevenly distributed time series since the meteorological
 95 conditions often prevented the accomplishment of one or both transects.
 96 Overall, TES was sampled 15 times and TAC 12 times.

97 TAC, located at the eastern entrance of the SoG, is the last MedS transect
 98 where the Mediterranean waters (MWs hereinafter) may be found as
 99 unmixed as in the interior of the Alboran Sea, the westernmost basin of the
 100 MedS. Further west, the enhanced turbulence associated with the tidal
 101 dynamics and the very hydrodynamics of the exchange (Weson & Gregg,
 102 1994; Sánchez-Garrido, et al., 2011) favour the mixing and erodes the
 103 specific θ -S characteristics of the different MWs participating in the outflow.

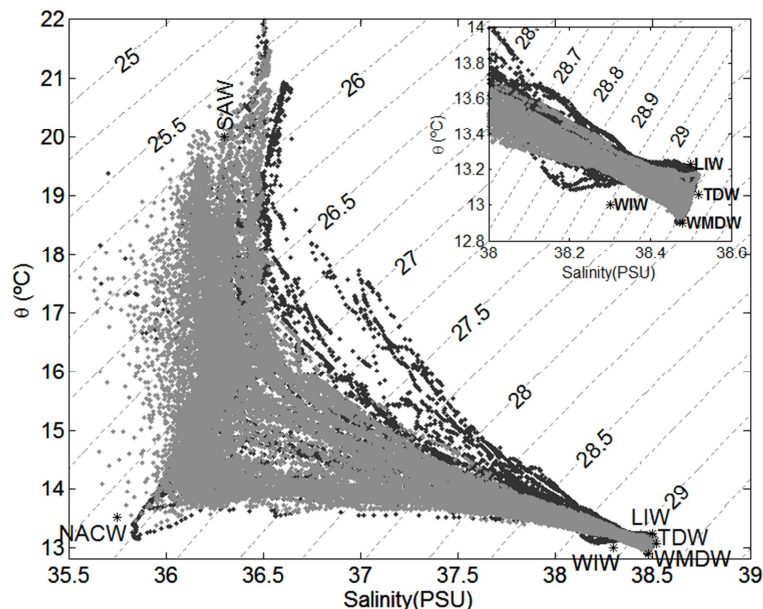
104 TES transect on the other hand lays along the western boundary of the SoG
105 and represents its last gateway for the MWs before they plunge down into
106 the Gulf of Cádiz and the Atlantic Ocean.

107 3. Data Processing

108 3.1. Definition of Water masses in the Strait of Gibraltar.

109 Beside the four MWs that can be detected in the outflow (LIW, WIW, TDW
110 and WMDW), two AWs, the Surface Atlantic Water (SAW) and North Atlantic
111 Central Water (NACW) shape the inflow. Therefore, a total of six water
112 masses may be involved in the exchange. In order to provide the necessary
113 inputs for the cluster analysis (Section 3.2), all they have to be defined by
114 certain hydrological characteristics that locate them in the θ -S diagram.
115 This identification is a previous step to quantify their influence, importance,
116 and distribution in the SoG.

117 There is no general agreement about the values characterizing each water
118 mass. Table 1 summarizes the information coming from different sources,
119 which differs slightly from one another due to the marked spatial and time
120 variability in the SoG. Along with this information, Table 1 shows the θ -S
121 characteristics assigned to each of the six water masses in this study, which
122 are located in the θ -S diagram of Figure 2.



123

124 Figure 2. θ -S diagram of the whole data set (GIC data in grey, INGRES data in black). The
125 locations of the water masses defined by the thermohaline properties showed in Table 1 are
126 marked by stars, with their acronyms aside. The inset is a zoom of the Mediterranean Water
127 zone of the diagram.

128 The noticeable seasonality of the SAW (Bray et al., 1995) caused by the
 129 heat exchange with the atmosphere coerced us to define two different θ
 130 values for this water mass, depending on when the measurements were
 131 collected (see Table 1). In summer months, the potential temperature
 132 representing this water was set to 19.7°C. If the maximum temperature
 133 found in the sampling exceeded 19.7 °C, this maximum replaced the
 134 $\theta=19.7^\circ\text{C}$ reported in Table 1.

135

Water mass	Author	θ (°C)	Salinity (PSU)	
SAW	(Bray, et al., 1995)	15.9 – 22.7	36.2 - 36.5	
	(Criado-Aldeanueva, et al., 2006)	16	36.4	
	GIC&INGRES	<i>March to June</i>	17	36.3
		<i>July to November</i>	19.7	36.3
NACW	(Bray, et al., 1995)	12.7 - 13.3	35.7 – 35.8	
	(Criado-Aldeanueva, et al., 2006)	11-17	35.6 - 36.5	
	GIC&INGRES	13.5	35.75	
LIW	(Smith, et al., 2008)	> 13.2	38.45 - 38.75	
	(Font, 1987)	13.3	38.5	
	(Parrilla & Kinder, 1985)	13.15 - 13.25	38.47 - 38.51	
	(Millot, 1999)	13.2 - 14.0	38.5 - 38.7	
	(García-Lafuente, et al., 2007)	13.22	38.56	
	GIC&INGRES	13.23	38.50	
WMDW	(Bray, et al., 1995)	12.8 – 12.9	38.4 – 38.5	
	(Salat & Font, 1987)	12.75 - 12.9	38.4 - 38.48	
	(Parrilla, et al., 1986)	13.15 - 13.25	38.47 - 38.51	
	(Fuda, et al., 2000)	12.70 - 13.03	38.40 - 38.50	
	(García-Lafuente J. , et al., 2007)	12.80	38.45	
	GIC&INGRES	12.90	38.48	
WIW	(Vargas-Yañez, et al., 2002)	12.5 – 13.0	38.1 - 38.3	
	(Smith, et al, 2008)	12.821	37.9 - 38.1	
	(Salat, et al., 1987)	12.5 - 13.0	38.1 - 38.3	
	(Ismail, et al., 2014)	<13.8	39.9 - 38.2	
	(Ribó, et al., 2015)	12.7	38.1	
	GIC&INGRES	13	38.3	
TDW	(Millot, 2009)	13.0 - 13.1	38.48 - 38.51	
	GIC&INGRES	13.06	38.52	

136
 137
 138

Table 1. Historical values of the hydrological characteristics of the six water masses involved in the exchange through the SoG. Shaded rows highlight the pair of values used in this work.

139 3.2. Classification of the water masses: cluster analysis.

140 3.2.1 The cluster analysis

141 The cluster analysis is a mathematical tool used in this work to assess the
142 presence and prevalence of each of the water masses in the different
143 transects sampled in GIC and INGRES datasets. The cluster analysis is a
144 multivariate method that aims at classifying samples on the basis of a set of
145 measured variables. The method separates the dataset into groups, called
146 clusters, each cluster including samples that are more similar to each other
147 than to the items located into another cluster, according to a given
148 criterion.

149 After an initial classification of the samples (a first guess, defined by the
150 user in the present case), the inter-cluster and intra-cluster variance is
151 calculated, and a new distribution of the samples is proposed, which has to
152 maximize (minimize) a certain metric that define the similarity
153 (dissimilarity) within (between) the clusters. The algorithm iterates until it
154 converges. The technique has been widely used to classify hydrographical
155 datasets (Kim, et al., 1991; Warn-Varnas, et al., 2005; Hur, et al., 1998).
156 Classical clustering tends to give clusters with similar shape (Yan, 2005)
157 and the method is especially appropriate to discriminate water masses with
158 similar salinity and temperature variance. Unfortunately, this is not the case
159 in the SoG, where MWs range much more in temperature than in salinity
160 and AWs are largely variable in temperature, as was already remarked
161 regarding the SAW. This drawback has been overcome by including the
162 density anomaly (σ_θ) in the hydrological properties of each water mass,
163 which is computed directly from the sea water state equation. Adding this
164 new variable makes the model more reliable as it favours the realistic fact
165 that isopycnal prevails over diapycnal mixing, since a water particle with the
166 same θ -S distance to the centroid of two clusters will finally be linked to the
167 one with more similar σ_θ .

168 Shaded rows in Table 1 and symbols in Figure 2 give the θ -S pairs for each
169 of the six defined water masses, which are the centroids of the clusters.
170 While NACW, LIW, WMDW, WIW and TDW have fixed θ -S and, hence, σ_θ
171 values, the θ of the SAW changes depending on the time of the year.
172 Another remark concerns the WIW: due to its intermittency, this water
173 mass may or may not be detected in the SoG. For instance and according to
174 the zoom in the inset of Figure 2, no traces of WIW were detected during
175 the GIC campaign since the θ -S dots do not deviate towards the WIW

176 centroid. In these cases, WIW must not be included in the cluster analysis.
 177 Thus, previously to carry out the analysis, each CTD cast is carefully
 178 inspected to detect the WIW and in case that a convincing evidence of its
 179 presence is not found, this water mass is excluded from the analysis of the
 180 cast in order to avoid the distortion of the results.

181 The metric usually employed to calculate the similarity between the
 182 observation and the cluster is the squared Euclidean distance

$$D_{o,c} = \sum_{i=1}^n (\vec{P}_o(i) - \vec{P}_c(i))^2 \quad [1]$$

183 where $D_{o,c}$ is the distance between a sample at a given longitude, latitude
 184 and depth, denoted by the vector $\vec{P}_o(\theta, S, \sigma_\theta)$, and a cluster centroid, denoted
 185 by the vector $\vec{P}_c(\theta_c, S_c, \sigma_{\theta_c})$, which represents a certain water mass. The θ - S -
 186 σ_θ variables have been previously normalized. Index i stands for the i -th
 187 variable of the sample (or cluster vector), thus $n = 3$ in eq. [1].

188 The fraction of a given water mass in a given sample "o", F_{o,c_j} , is determined
 189 by

$$F_{o,c_j} = \frac{D_{o,c_j}^{-1}}{\sum_{j=1}^m D_{o,c_j}^{-1}} \quad [2]$$

190 using the distance D_{o,c_j} of the sample to the centroid of cluster j ($j = 1, \dots, m$).
 191 Distances have been normalized ($\sum_{j=1}^m D_{o,c_j}^{-1} = 1$) to have all them lying
 192 between 0 and 1. Index m is the number of cluster in the analysis, which
 193 can be 6 or 5 depending on whether or not WIW is included.

194 3.2.2 Sensitivity of the method

195 As long as the method to classify the samples in clusters depends on the
 196 cluster centroids, this is, on the definition of the water masses, its
 197 sensitivity must be tested. This will be achieved by computing the
 198 percentage of samples (measurements) that change from one cluster to
 199 another when the centroid is slightly modified.

200 Table 2 shows the sensitivity analysis for transect R2 (see Figure 1) when
 201 the θ of the LIW was modified between 13.196-13.264 °C, a 20% of the
 202 maximum difference with the TDW potential temperature, which is its
 203 nearest water mass.

204 The number of samples that were removed from their initial cluster does not
 205 reach the 5% in the worst case, which corresponds to θ_{LIW} decreasing by
 206 0.034 °C (first row in Table 2). In this case, LIW cluster increases at the
 207 expense of WMDW and TDW, which remove samples near equally. On the
 208 contrary, when θ_{LIW} is raised from its chosen reference, nearly all samples
 209 leaving LIW go to WMDW cluster while a smaller proportion moves toward
 210 the TDW cluster, there is also a negligible portion that moves from NACW to
 211 LIW. Overall, Table 2 supports the robustness of the method, as no
 212 significant changes occur if the centroids are moved within a realistic range.
 213 Similar tests have been carried out by moving other centroids with the
 214 same results.

$\Delta\theta_{LIW}$	Samples modified (%)	WMDW to LIW (%)	TDW to LIW (%)	LIW to TDW (%)	LIW to WMDW (%)	NACW to LIW (%)
-0.034	4.77	2.14	2.63	0	0	0
-0.019	2.44	1.43	1	0	0	0
-0.004	0.64	0.46	0.18	0	0	0
+0.011	1.40	0	0	0.367	1	0.03
+0.026	2.17	0	0	0.458	1.7	0.03

215 Table 2. Sensitivity analysis of the clustering algorithm when the θ assigned to the LIW
 216 centroid is slightly changed. The variation of θ corresponds with a 20% of the difference
 217 between θ_{LIW} and the nearest water mass to LIW, θ_{TDW} . The first column shows the variation
 218 of LIW temperature over its assigned value of $\theta=13.23^\circ\text{C}$. The second column shows the
 219 percentage of samples that changed membership from one cluster to another. Columns third
 220 to sixth specify the implied clusters in the new distribution. The sum of these four columns
 221 has to coincide with column two.

222 Regardless of the accuracy of the θ -S pairs defining each cluster centroid
 223 and as long as the paper is comparing data collected in the same region
 224 with the aim of investigating the spatial-temporal variability of the water
 225 masses, the key issue is to maintain the same centroids throughout the
 226 analysis. Even when the exact proportions of the involved water masses
 227 depend slightly on the centroids choice, their relative variations from place
 228 to place and/or from time to time will be representative of the investigated
 229 variability.

230

231 4. Results

232 4.1. GIC dataset

233 The tidal variability in the SoG, subdued by semidiurnal frequencies, makes
234 the water masses pattern be dependent on the time of the tidal cycle when
235 the transect was accomplished (García-Lafuente et al., 2007) and the tidal
236 phase during which the sampling was carried out must be specified for each
237 transect. This information is provided by the sea level oscillation in Tarifa
238 (see Figure 1). In this regard, it is interesting to remind that the barotropic
239 semidiurnal tide in the SoG behaves like a standing wave (Garcia-Lafuente,
240 et al., 1999, 2000) and that the tidal flow goes westwards during the rising
241 tide (low to high water, or flood tide) and eastwards during the falling tide
242 (high to low water, or ebb tide). On the other hand, the GIC sampling was
243 accomplished during a relatively short period of time (4th to 6th of July,
244 2012). In some sense, the observations are synoptic for lower frequency
245 fluctuations (subinertial or seasonal/interannual variability) and they should
246 reflect the water mass composition in the SoG during that period of time,
247 despite the tidal variability.

248 The results of the analysis of the GIC transects are presented from east to
249 west in Figure 3 and Figure 4. During this survey, no traces of WIW were
250 observed and the cluster analysis involved only five water masses: WMDW,
251 TDW, LIW, NACW and SAW.

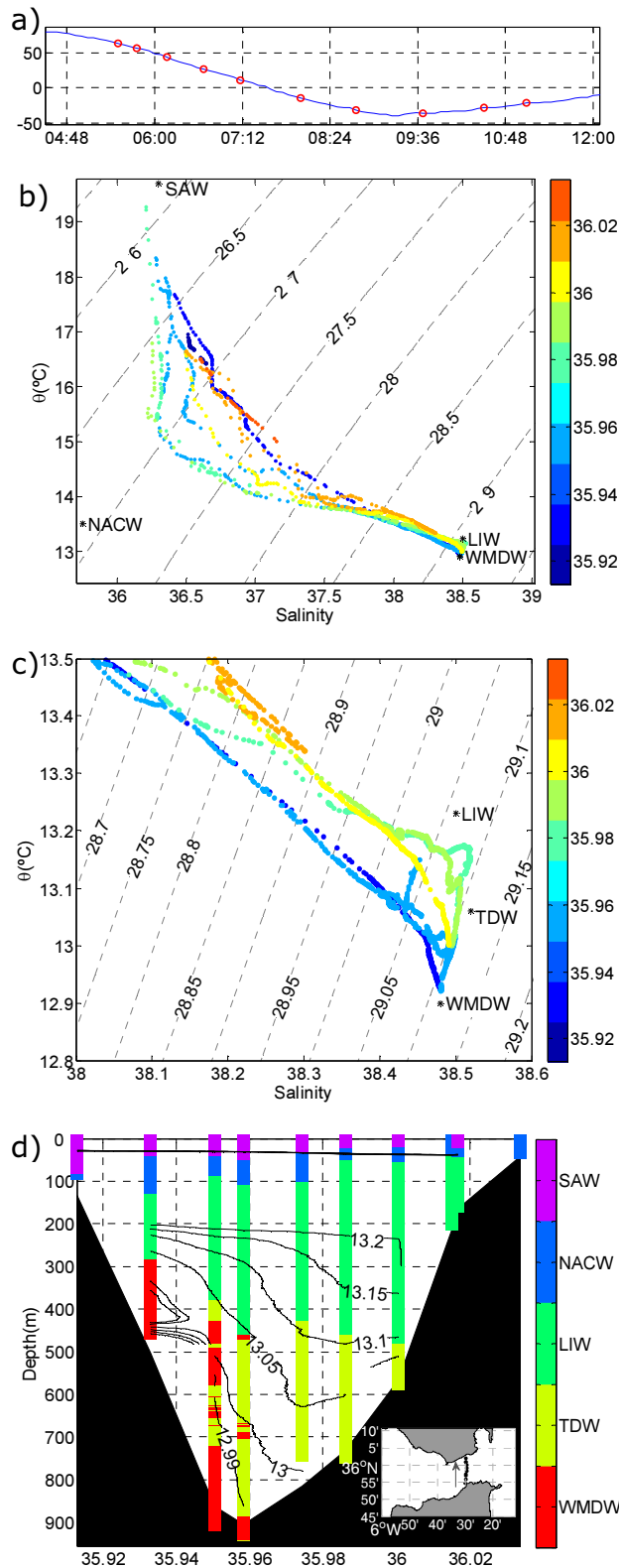
252 Figure 3 corresponds to the easternmost transect, R5, where the less mixed
253 MWs that enter the SoG from the MedS are expected to be found. The
254 transect was carried out from south to north with a CTD probe during the
255 ebb tide, the last station being completed shortly after the slack tide of low
256 water (Figure 3a). The θ -S values of the densest water sample were
257 12.92°C-38.48, which corresponds to WMDW (Figure 3c). Figure 3d shows
258 that this water stacks up in the south while the LIW layer is thicker in the
259 north, a spatial pattern that agrees with Parrilla et al. (1986) and Naranjo,
260 et al. (2012). Millot (2014) pointed out that LIW (and also TDW to some
261 extent) is pushed to the north due to the Coriolis force because it is lighter
262 and moves faster than WMDW. The latter is compelled to flow attached to
263 the southern shore preferably, where the incoming AWs, NACW in
264 particular, are accumulated due to the Coriolis effect too (Figure 3d). Such
265 a distribution facilitates the mixing of WMDW with AWs in the south part, a
266 fact reflected by the mixing lines of the southernmost stations of the
267 transect, which head directly towards the AWs region from the vicinity of

268 the WMDW centroid (Figure 3c). This is not so for the stations located further
269 north in the transect where the mixing lines bend towards the LIW centroid
270 before heading towards the AWs, showing that it is mainly the LIW and not
271 the WMDW nor the TDW that mixes with the AWs.

272 The remaining transects discussed below were sampled with the MVP. The
273 way the instrument samples the water column results in shorter times to
274 complete a transect and higher spatial resolution (Figure 4). However, the
275 maximum sampled depth is less than the one reached by CTD.

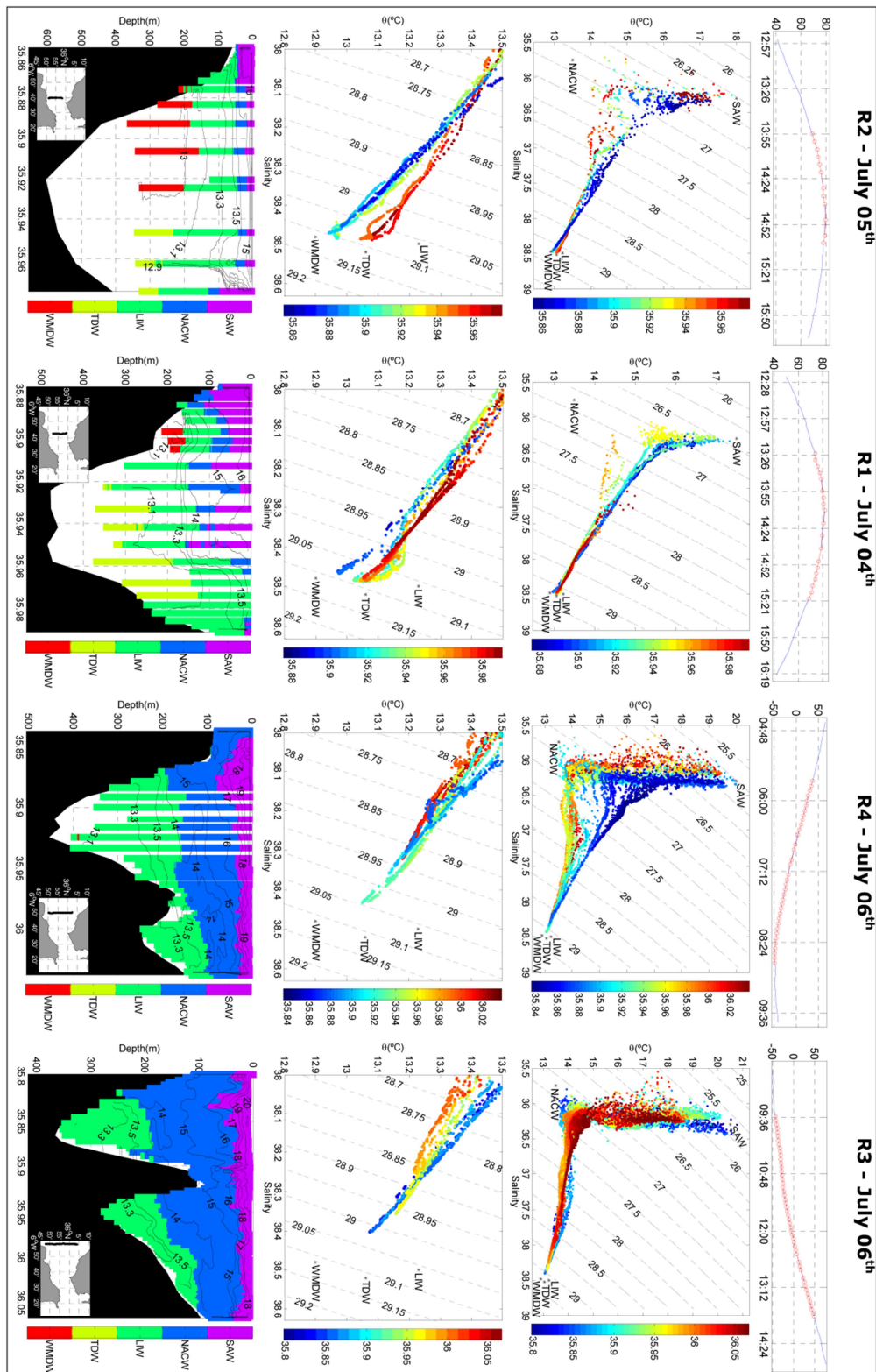
276 Next transect to the west is R2 (panels in column I of Figure 4). It is located
277 to the east of CS so that the water masses have not been exposed yet to
278 the strong mixing happening in the sill area (Wesson and Gregg, 1994;
279 Sanchez Garrido et al., 2011). Moreover, it is not far from R5 and no
280 significant differences are thus expected. That is the case for AWs, which
281 depict a similar pattern (Figure 4-I-d). However, WMDW and TDW rise to
282 shallower depths, a clear effect of tides: R2 transect was sampled during
283 the rising tide and near the high tide (Figure 4-I-a) when the interface
284 between MWs and AWs moves up in the vicinity of Tarifa (Bryden et al,
285 1994; Sánchez-Román, et al., 2012). The situation is just the opposite of
286 R5 sampling. The most interesting feature, however, is the spatial
287 differentiation of the MWs (Figure 4-I-c,d) with WMDW occupying the
288 southern part and TDW and LIW the northern area, although the latter is
289 found at intermediate depths all over the transect.

290 The following transect R1 is still east, although near, of CS (R1, Figure 4-
291 II). It is also close to R2 so a certain similarity between them is expected.
292 But differences are apparent in the south due to the inversion of the tidal
293 flow. R2 was accomplished from south to north and the southern stations
294 were sampled ~ 1 h before the high tide during the flood tide (Figure 4-I-a),
295 while R1 was accomplished from north to south with the stations in the
296 south were done during the ebb tide ~ 1 h after the high tide (Figure 4-II-a).
297 During this tidal phase the interface between AWs and MWs sinks nearby CS
298 (Sánchez-Román, et al., 2008), giving rise to a considerably thicker AWs
299 layer (Figure 4-II-d). The northern half of both sections were sampled
300 under similar tidal conditions near the high water, when the interface is at
301 its shallowest position (Sánchez-Román, et al., 2012), and show similar
302 accumulation of LIW and TDW and a very thin layer of AWs. The spatial
303 differentiation showed in Figure 4-I-c for R2 is easily recognisable in Figure
304 4-II-c for transect R1 as well, which is another remarkable similarity.



305
 306
 307
 308
 309
 310
 311
 312

Figure 3. (a) Tidal oscillation at Tarifa displaying the time of the CTD casts (red dots) in the R5 transect, which was accomplished from south to north. (b) θ -S diagram showing the CTD data of the R5 transect. The centroids of the different water masses are marked with asterisks and the colour scale on the right identify the different water casts by their latitude. (c) Zoom of the MWs area of the θ -S diagram. (d) Results of the cluster analysis where each colour represents the cluster associated with a water mass according to the legend on the right.



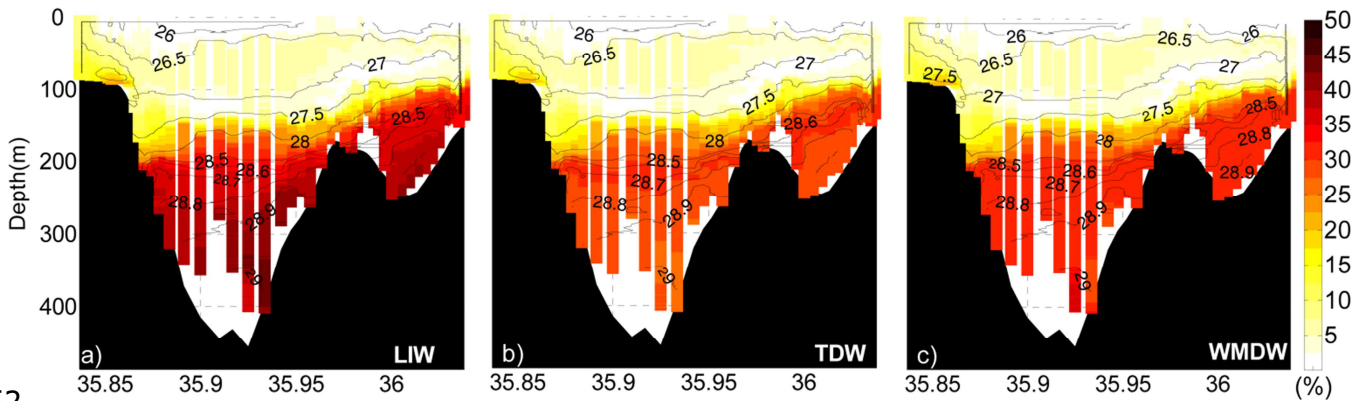
313
 314
 315
 316
 317
 318
 319
 320
 321

Figure 4. Zonal evolution, from East to West, of the thermohaline properties for the different water masses involved in the exchange at the SoG. The figure is divided in four columns named I, II, III and IV and each of them is subdivided in rows. The upper row, (a), shows the sea level during the sampling of each transect, with the red circles indicating the time of the different casts. The second row, (b), displays the θ -S diagram of the whole section. The names and locations of the defined water masses are indicated. The third row, (c), is a zoom of the θ -S diagram that focuses on the MWs. Finally, the last row, (d), shows the classification of the water masses in the section provided by the cluster analysis.

322 Next transect to the west is R4 (Figure 4-III), which is already west of CS.
323 The θ -S diagram shows two noticeable differences with regards to the three
324 previous transects. Firstly, the θ -S curves bend towards the NACW centroid,
325 implying a much greater impact of this water mass that now spreads
326 downwards to 200m depth in the south (Figure 4-III-d). Secondly, the
327 spatial differentiation of the MWs has disappeared and now they nearly lay
328 along a single mixing line. This is an obvious outcome of the strong mixing
329 in the Tangier basin (Sánchez-Garrido et al., 2011) which makes the MWs
330 lose its specific identity to a great extent. The cluster algorithm only returns
331 one kind of MWs in this transect, LIW in this case, which is somewhat
332 misleading in view of the θ -S diagram in Figure 4-III-c. Therefore, it
333 requires clarification. The algorithm situates the water samples in a cluster,
334 which is the one with the greater percentage of the water mass defined by
335 the corresponding centroid. According to the chosen metrics (Eq. 1 and 2),
336 the deep water samples in this transect (and also in the next one, R3,
337 commented below) have similar proportions of the three MWs but a slightly
338 higher proportion of LIW (Figure 5). Should we have displaced any of the
339 centroids of the MWs by a tiny distance, the algorithm would have possibly
340 returned a different prevailing cluster. The reasonable conclusion is that the
341 MWs are hardly distinguishable once the Mediterranean outflow has passed
342 CS and that the sensible option is to speak of a unique "Mediterranean
343 water".

344 On the other hand, it is noteworthy here the effect of adding σ_θ to the
345 metrics. Should it not be included, all the deep water would have been
346 classified as TDW with an overwhelming percentage, as can be easily
347 deduced from Figure 4-III-c. Its inclusion in the metrics makes the
348 algorithm work more realistically in the sense that the actual sampled water
349 is more likely to be the result of local mixing between LIW and WMDW (and
350 TDW as well) than the outcome of the individual contribution of TDW.

351



352
353
354
355

Figure 5. Percentage of the MWs in transect R4 (Figure 4, column III). The sum of the three contributions gives the 100% in the Mediterranean layer. The colour scales go from 0 to 50% for the sake of clarity. Contours represent the σ_t .

356 The westernmost section R3, located in the western exit of the SoG, shows
357 large similarity with the previous one. The fading out of the spatial
358 differentiation of the MWs already detected in R4 is now more evident
359 (Figure 4-III-c), and so it is the prevalence of the NACW in the Atlantic
360 layer (Figure 4-III-d). Mixing lines are organised along two well-depicted
361 directions, from MWs to NACW, and from NACW to SAW (Figure 4-III-b),
362 indicating that direct mixing of MWs with SAW does not happen any longer.
363 Notice that this mixing can be partially detected in the previous transect R4
364 (Figure 4-III-b), this feature being almost the only difference among the
365 two westernmost transects. The commentaries about the outputs of the
366 cluster algorithm regarding the MWs made for R4 still apply in this transect.

367 The previous discussion has focussed on the spatial evolution of the
368 different water masses as they flow through the SoG. Table 3 presents the
369 θ -S values of the densest water mass sampled in every transect in order to
370 illustrate the transformation of the MWs in its path to the Atlantic Ocean. It
371 also displays the coldest sample with salinity lower than 36.5, which is the
372 best example representing NACW at each transect, in order to show the
373 alteration of this water in its way towards the MedS. In the case of the
374 MWs, θ increases and S decreases towards the west, the greatest jumps
375 occurring between the transects R1 and R4 that surround CS, thus stressing
376 the importance of this area as a source of turbulence (Weson and Gregg,
377 1994; Sanchez-Garrido et al., 2011). The opposite applies for the NACW,
378 since both θ and S tend to increase as the water flows eastward. Once
379 again the main changes happen in the surroundings of CS, although the
380 rising of θ and, in particular, of S still continues from R2 to R5.

381

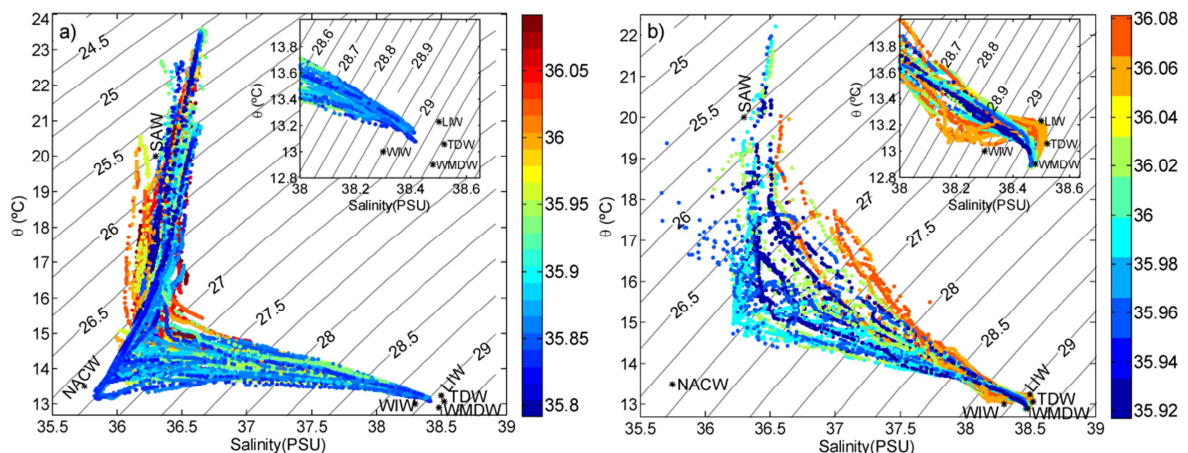
382

		R5	R2	R1	R4	R3
		(east)			(west)	
MWs	θ ($^{\circ}\text{C}$)	12.92	12.94	12.97	13.05	13.07
	S (psu)	38.48	38.47	38.46	38.43	38.40
NACW	θ ($^{\circ}\text{C}$)	14.72	14.03	14.45	13.37	13.64
	S (psu)	36.48	36.15	36.24	35.95	36.03

383 Table 3. The two first rows show the potential temperature and salinity, respectively, of the
 384 densest sample observed in the transect (MWs block). Third and fourth rows show the
 385 potential temperature and salinity of the coldest sample with salinity less than 36.5 (NACW
 386 block). The different columns correspond to the different transects, which have been
 387 organised from east (R5) to west (R3), see Figure 1 for details.

388 4.2. INGRES

389 Transects TES and TAC (see Figure 1) have been sampled now and again
 390 since year 2004 and they are more regularly accomplished since year 2011.
 391 Figure 6 presents the θ -S diagrams of both transects that confirms the
 392 already mentioned evolution of the water masses as they progress through
 393 the SoG: the erosion of the NACW signal from TES (west) to TAC (east) and
 394 the fading of the spatial differentiation between MWs from TAC (east) to
 395 TES (west). In particular, the reddish colours in the inset of Figure 6b
 396 illustrates the fact that LIW, WIW and TDW flow preferably across the
 397 northern half of the SoG while the WMDW flows attached to the southern
 398 slope. The inset of Figure 6a shows how the former pattern is lost at TES.



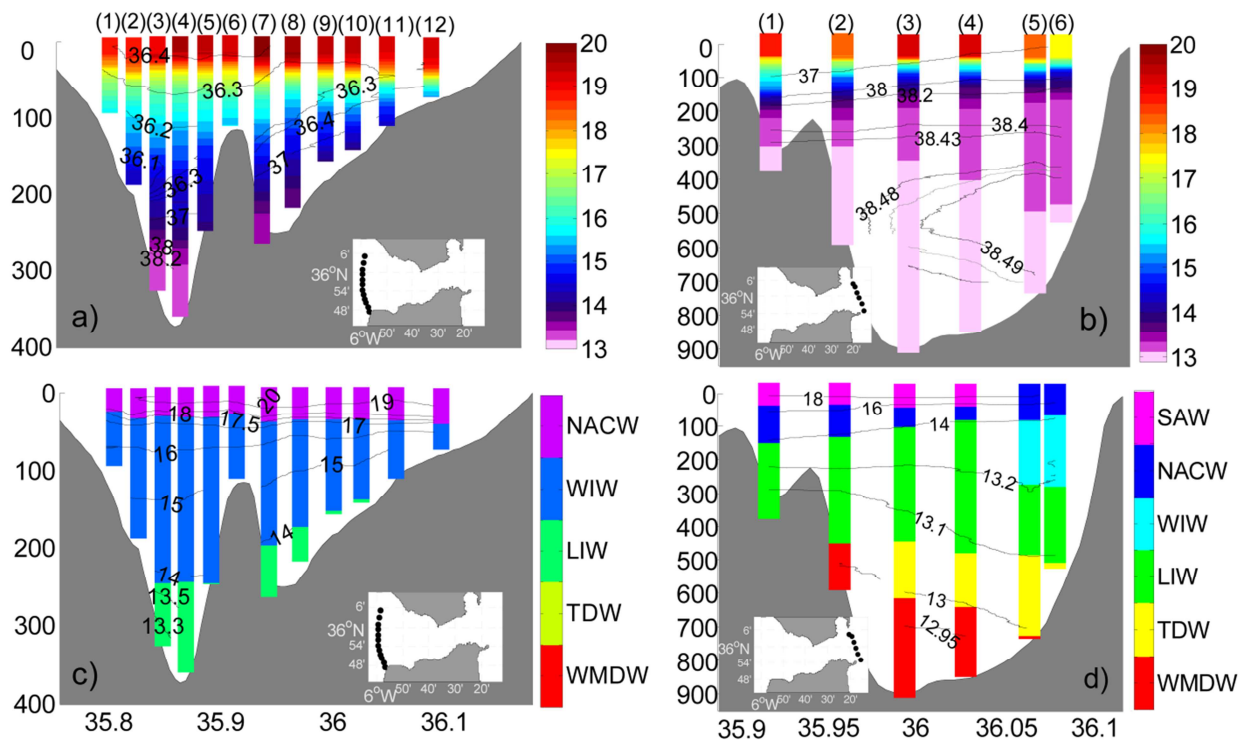
399 Figure 6. θ -S diagram showing the CTD data collected at TES (a) and TAC (b) transects
 400 during the INGRES project from 2004 up to the present. The colour scale indicates latitude.
 401 Black stars mark the θ -S pairs of the water masses involved in the exchange (see Table 1).
 402 The insets zoom in the Mediterranean water zone of the diagram.
 403

404 4.2.1. Spatial distribution

405 Figure 7a-b show the mean potential temperature and salinity distributions
406 at TES and TAC sections, respectively, which have been obtained by
407 averaging all the transects collected within INGRES. Figure 7c-d show the
408 results of applying the cluster analysis to the same sets of data.

409 At TES, the cluster analysis only detects three water masses (Figure 7c), in
410 agreement with the results obtained from the GIC data in this area. The
411 bottom layer is occupied by the MWs, which the cluster analysis identifies as
412 LIW (the same cautionary comments on the identification of MWs as LIW
413 made for R4 transect in the previous Section apply here). These MWs,
414 whose averaged salinity is ~38.2 with maxima of 38.4, flow mainly through
415 the southern channel below 250 meters, the volume flowing through the
416 northern channel being much smaller. NACW is the prevailing water mass,
417 occupying a layer from 50 to 250 meters in the southern channel (Figure
418 7c). Obviously not all this layer is NACW. It includes its mixture with the
419 overlying (SAW) and underlying (LIW) waters, with the NACW entering in
420 greater proportion than the others. Actually, Figure 7a shows a core of
421 minimum salinity around 150-200m depth in the southern channel, which
422 would be the depth where the purest NACW is flowing.

423 The cluster analysis at TAC transect shows the averaged spatial distribution
424 of the six water masses involved in the exchange (Figure 7d). Contrary to
425 GIC, INGRES data recorded WIW, which now is identified flowing attached
426 to the north shore just below a very thin layer of NACW. The remaining
427 MWs display the same spatial pattern as in GIC: the WMDW, easily
428 identified by $\theta < 13^{\circ}\text{C}$ in Figure 7d, resides in the deepest layer and
429 preferably stacked up in the southern half of the transect; the TDW and
430 LIW, which appear as a salty wedge encircled by the isohaline 38.485 (grey
431 line in Figure 7b), occupy an intermediate layer that thickens to the north.
432 Any of these MWs is saltier ($S > 38.4$, see Figure 7b) than the rather mixed
433 MW at TES, a result that can only be explained by the entrainment of AW by
434 the Mediterranean outflow west of Camarinal Sill, as discussed in García
435 Lafuente et al. (2011). The two AWs are at the top of the water column in a
436 layer that thickens from ~100m in the north to ~150m in the south. The
437 presence of NACW is appreciably reduced as it experiences a marked mixing
438 with respect to the TES transect (compare Figure 7c and Figure 7d). The
439 blue colour identifying NACW in Figure 7d must be then interpreted as the
440 sample being closer to NACW than to any other water mass and not as if it
441 were aside the point marking the pure NACW.



442
443
444
445
446
447

Figure 7. Averaged potential temperature (colour scale) and salinity (labelled contours) of the whole dataset collected at TES (a) and TAC (b). Panels (c) and (d) show the distribution of water masses in these transects provided by the cluster analysis. Contours display the potential temperature. Insets show the location of the cast in each transect.

448

4.2.2. Temporal fluctuations in the core of the water masses

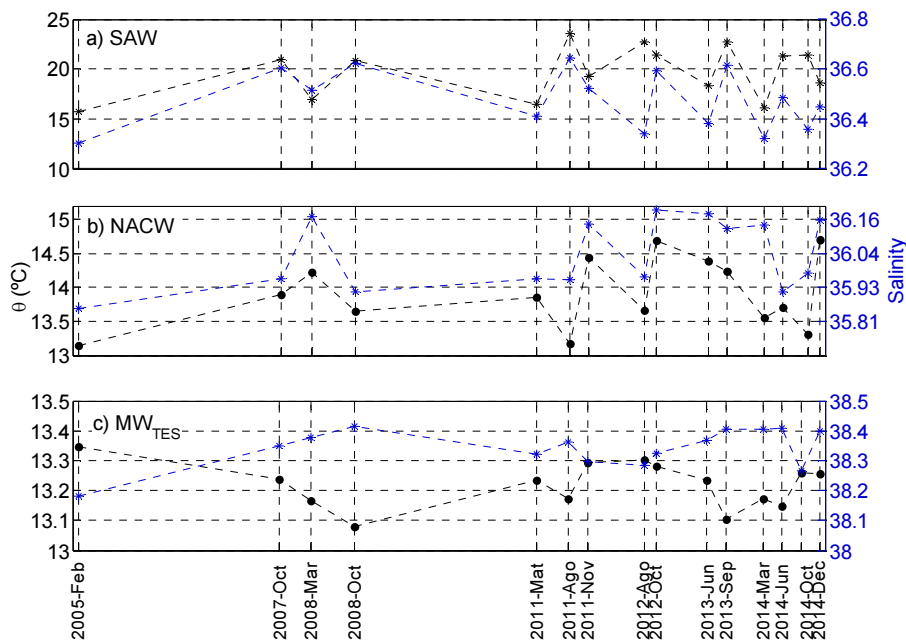
449
450
451
452
453

This section addresses the time variability of the thermohaline characteristics found in INGRES data. To this aim, we have selected representative samples of each water mass with the same criterion for a given transect, although the criterion may change slightly from the west (TES) to the east (TAC) transect, as explained below.

454
455
456
457
458
459
460
461
462
463
464
465

At TES, only three water masses have been worked out: SAW, NACW and what we shall refer to as MW_{TES} , a mixing of all the MWs that are no longer distinguishable. The representative sample of SAW and NACW were the warmest and freshest ones, respectively, while MW_{TES} was represented by the saltiest sample. Figure 8 displays the selected points for each cruise. As expected, seasonal fluctuations is the obvious characteristic of SAW (Figure 8a), with warmer and also saltier water during the summer and early-autumn months. It is the most variable water mass, as can be deduced from Table 4 as well. The NACW (Figure 8b) shows some seasonality, which consists in a diminution of θ in summer months. It would be associated with the upwelling-favourable winds in the Gulf of Cádiz, which uplift deeper and, hence, colder NACW, making it available for the inflow during the upwelling

466 season (Criado-Aldeanueva, et al., 2006; Folkard, et al., 1997). A positive
 467 salinity trend is visible in Figure 8b, only interrupted during the second part
 468 of year 2014. The MW_{TES} (Figure 8c) is the least variable water mass in this
 469 transect. Temperature and salinity display a rather specular pattern,
 470 suggesting that colder (warmer) water is simultaneously saltier (fresher),
 471 giving thus rise to enhanced fluctuations of density. MW_{TES} does not show a
 472 clear seasonality, neither a short-term trend, although from year 2012
 473 onwards the salinity is greater than the mean of the series (38.34, see
 474 Table 4).



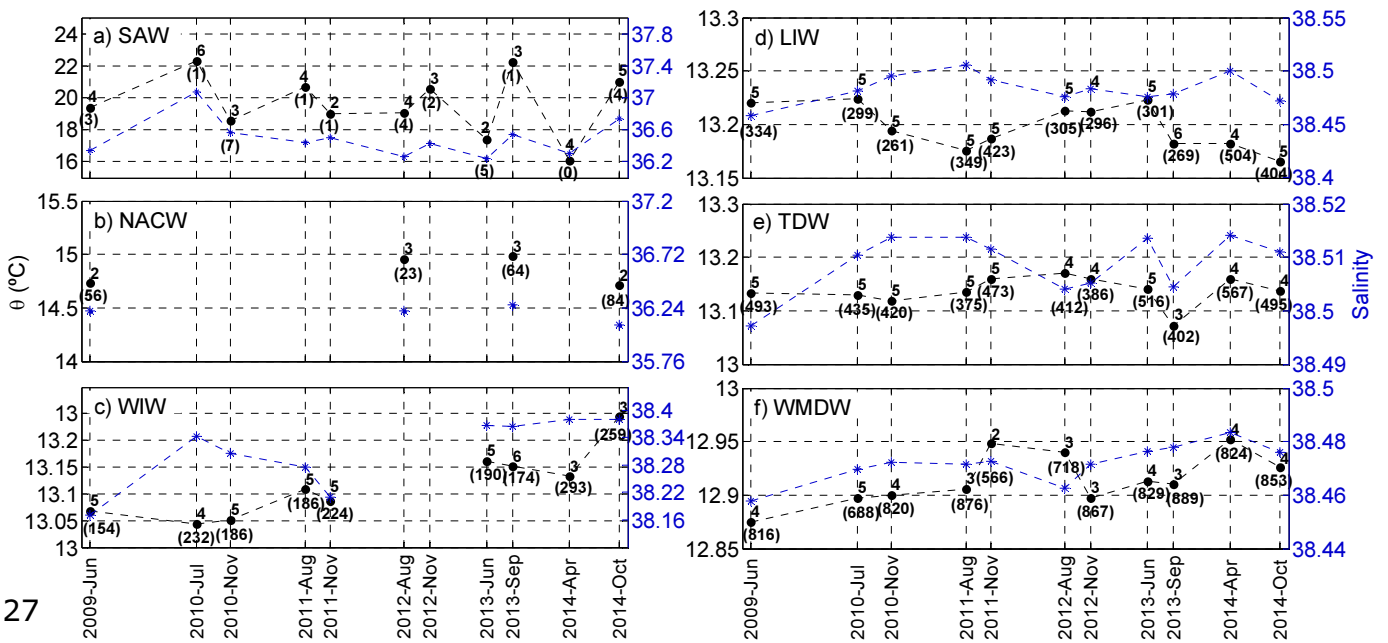
475
 476 Figure 8. Potential temperature (left axis, black points) and salinity (right axis, blue stars) of
 477 the water masses addressed in TES: Panel (a) is for SAW, panel (b) is for NACW, and panel
 478 (c) is for MW_{TES} . See text for details.

479 A similar analysis has been conducted at TAC, now addressing the six water
 480 masses. The criterion to define each water mass must be selected carefully,
 481 as the four MWs detected in this transect have only very small thermohaline
 482 differences. The SAW is still selected as the warmest sample. The NACW
 483 has been widely altered by mixing and the freshest water criterion followed
 484 at TES may be not applicable at TAC (see θ -S diagram of Figure 6b). Even
 485 more, the mixing could have been so important that speaking of NACW
 486 makes no clear sense. Thus, we only admit the presence of NACW if a clear
 487 minimum of salinity with respect to the overlying SAW is observed in the
 488 vertical profile, otherwise we ignore this water mass, even if
 489 temperature/salinity dots in the θ -S diagram bend gently towards the mark
 490 representing the NACW. Regarding the MWs, WMDW is determined as the
 491 coldest sample, TDW as the saltiest one, and LIW as the warmest whenever
 492 its salinity exceeds 38.4. As for the WIW, it is identified as the coldest

493 sample between $\sigma_\theta=28.0$ and $\sigma_\theta=29.0$ (Millot, 2014), provided that it is
494 visually detected in the θ -S diagram previously (that is, whenever the
495 relative minimum around the WIW position in the diagram is positively
496 identified, see inset in Figure 6b).

497 Figure 9 shows the series of these representative samples at TAC transect,
498 which are displayed along with the depth where the sample was found (in
499 brackets) and the location of the profile (see labels on top of Figure 7). The
500 seasonality of SAW is recognisable at TAC transect as well (Figure 9a). As
501 for the NACW, it was positively identified only 4 out of 11 times (Figure 9b).
502 In all these occasions its core mass always found in the southern casts
503 (casts 2 or 3) at depths between 20 and 85m, quite shallower than at TES,
504 where the NACW core was between 150 and 200m (Figure 7a).

505 Regarding MWs, except for year 2012 when WIW was not observed, the
506 four water masses were positively identified during all cruises. The lightest
507 one is the WIW, which is at the top of the Mediterranean layer between 150
508 and 260m and it is detected in casts near the northern shore, in agreement
509 with Figure 7d. April 2014 was the exception as the WIW sample was
510 detected deeper (305m) and shifted to the south (cast 3), a situation that
511 apparently extended until October 2014. LIW layer is beneath the WIW.
512 Despite being spread out through the whole transect (Figure 7d), its core is
513 found in the northern part, usually at the position of cast number 5 (Figure
514 9d) at depths between 260 and 300m. April and October 2014 were again
515 the exception, the LIW core being noticeably deeper. Curiously, warmer and
516 fresher LIW was detected in 2012, coincidentally with the absence of WIW
517 in the SoG. TDW is observed beneath the LIW between 370 and 500m with
518 preference to be detected close to the northern coast (casts 4 and 5),
519 according to Figure 9e. Once again April 2014 show an anomalously large
520 depth of the TDW core (567m). Finally, the densest WMDW occupies the
521 deepest layer with its core showing up close to the southern shore (casts 2
522 to 4) and always deeper than ~700m except for November 2011, when it
523 was detected at 568m in cast number 2 (Figure 9f). An absolute minimum
524 of θ and S is observed in June 2009, which could be the signature of an
525 exceptional event of deep water formation in the Gulf of Lion during this
526 year (Salat, et al., 2010).



527

528 Figure 9. Potential temperature (left axes, black dots) and salinity (right axes, blue asterisks)
 529 of the water samples representing each water masses at the TAC transect (see text for
 530 details). Numbers 1 to 6 aside the symbols indicate the cast were the samples were
 531 detected, according to the labels on top of Figure 7. Numbers within brackets display the
 532 depth of the sample (in meters from the surface).
 533

	TES		TAC		TES		TAC	
	$\bar{\theta} \pm \sigma$ (°C)	Trend (°C/year)	$\bar{\theta} \pm \sigma$ (°C)	Trend (°C/year)	$\bar{S} \pm \sigma$ (psu)	Trend (psu/year)	$\bar{S} \pm \sigma$ (psu)	Trend (psu/year)
SAW	19.76±2.60	0.28	19.74±1.80	<i>0.18</i>	36.47±0.12	0.0047	37.15±0.08	<i>0.026</i>
NACW	13.91±0.51	0.05	14.84±0.14	-	36.03±0.12	0.017	36.19±0.07	-
WIW	-	-	13.11±0.06	0.030	-	-	38.31±0.07	0.031
MW _{TES} /LIW	13.22±0.07	0.0035	13.20±0.02	<i>-0.0064</i>	38.34±0.06	0.0087	38.48±0.01	<i>9x10⁻⁴</i>
TDW	-	-	13.13±0.03	<i>9.3x10⁻⁴</i>	-	-	38.51±0.005	<i>0.001</i>
WMDW	-	-	12.91±0.02	0.0089	-	-	38.47±0.07	0.003

534
 535
 536
 537
 538
 539
 540
 541
 542
 543

Table 4. Mean values with standard deviation and trends of the potential temperature and salinity data displayed in Figure 8 and Figure 9. TES (shaded columns) correspond to the western exit of the Strait where MWs are no distinguishable and, therefore, a unique MW, denoted MW_{TES}, is specified (see text for details). Trend values in bold indicate that the trend is significant at the 95% significance level, while values in italics mean a non-significant trend at this level. Trends for NACW at TAC have not been computed since only four points were available.

544 5. Discussion and conclusions

545 The present study had the twofold objective of depicting the spatial
546 distribution of the water masses participating in the exchange through the
547 SoG and investigating the time variability of this pattern during the last
548 years. An intensive oceanographic survey carried out in summer 2012 (GIC
549 data) allowed us to address the first objective and the rather systematic
550 CTD monitoring of two specific transects at both ends of the SoG (INGRES
551 data) made it possible the analysis of the time variability.

552 A cluster analysis was performed on GIC data to classify the water samples.
553 Of all water masses reported in Table 1, the WIW was not detected and
554 therefore it was excluded from the analysis. Also, after examining the five
555 GIC transects and scrutinizing the zoomed θ -S diagrams of Figure 3 and
556 Figure 4, it is questionable the inclusion of the TDW in the algorithm. If it is
557 included the outcome of the analysis for the transects located east of CS
558 provides a pattern with the LIW and TDW occupying preferably the northern
559 part and the WMDW attached to the south (Figure 3d and Figure 4-I-II
560 panels d). It is in good agreement with the previous study by Millot (2014),
561 who put forward that TDW flowing over the bottom piled up against the
562 northern half of the SoG. Indeed, if we remove TDW from our analysis the
563 samples which will correspond with TDW are divided between WMDW and
564 LIW, with the samples incorporated to the LIW (WMDW) being located to
565 the centre-north (centre-south) of the transect, without modifying heavily
566 the distribution of Figure 7(not shown).

567 West of CS, the AWs are well differentiated but the MWs are not any longer
568 The cluster analysis only outputs a water mass, LIW in all cases, a result
569 somewhat misleading as the proportion of all the MWs in the samples is
570 very alike (Figure 5). It is just because the proportion of LIW is slightly
571 greater that the analysis ascribes the samples to the LIW cluster. Our
572 interpretation, however, is that the intense mixing underwent by the MWs
573 flowing west over CS blurs out their specific characteristics, leaving a rather
574 well mixed water that we have denoted by MW_{TES} . This is the water making
575 up the Mediterranean outflow in studies dealing with the Eastern North
576 Atlantic Ocean.

577 Overall, the most significant result of the analysis of GIC data is the great
578 erosion observable from west to east for the NACW and, in the opposite way
579 for the MWs (Figure 4 panel b and c), which lose its specific identity. Both
580 outcomes are a consequence of the outstanding mixing driven by tides that

581 takes place in the Camarinal sill surroundings (Weson and Gregg, 1994;
582 Sanchez-Garrido, et al., 2013).

583 The same cluster analysis has been performed on the whole set of INGRES
584 data at TES and TAC transects (Figure 7) with similar results. The main
585 difference is the presence of WIW among the MWs in the eastern transect in
586 9 out of 11 cruises, which shows up embedded between the LIW and the
587 AWs flowing close to the northern shore. Nevertheless, the goal of the
588 INGRES data analysis is the investigation of the time variability, for which
589 we have devised a criterion to identify the most representative samples of
590 each of the water masses involved in the exchange during every cruise
591 (Figure 8 and Figure 9). Mean values and trends during the period covered
592 by the observations are summarized in Table 4. Mean values at the different
593 transects merely inform about spatial variations and reflect the already
594 discussed changes suffered by the NACW in its path to the MedS as well as
595 the important mixing undertaken by the MWs after passing Camarinal sill.
596 Interestingly the mean value of MW_{TES} potential temperature at the western
597 transect (TES) is greater than any of the MWs mean values at the eastern
598 transect (TAC), which implies that a small proportion of NACW must be
599 involved in the MW_{TES} mixing. Salinity mean values also require the
600 participation of NACW in the mixing (García-Lafuente et al., 2007).

601 The marked seasonality of the SAW, and the NACW to some extent, along
602 with the intermittent sampling of the transects make the trends reported in
603 Table 4 be very uncertain for the AWs (notice that trends for NACW are not
604 computed at TAC due to the very small number of samples available).
605 Apparently, NACW shows a tendency to increase its salinity from 2011
606 onwards at TES (Figure 8b), although the drop by the summer of year 2014
607 would deny this conclusion. Actually, the trend reported in Table 4 for this
608 water is non-significant at the 95% confidence level. On the other hand, the
609 fact that the seasonal expected drop of salinity during the previous summer
610 (June 2013 cruise, Figure 8b) had not taken place supports the salinity
611 increase scenario, which otherwise would not be so apparent.

612 Trends in MWs are better investigated at the TAC transect. Six-year
613 observations are obviously insufficient to speak of long-term trends, but
614 some of the short-term trends that are drawn from our reduced dataset
615 may be related to trends already mentioned in the literature (Borghini, et
616 al., 2014). During the studied period, neither the LIW nor the TDW show
617 significant trends (Table 4), whereas both WIW and WMDW exhibit positive
618 temperature and salinity trends, which are more pronounced for the former

619 (Table 4). While the seasonality, intermittency, relatively small volume, and
620 intermediate nature of the WIW formed in the northwest area of the
621 Western MedS raise questions about the reaching and consequences of their
622 estimated trends, the trends found for the WMDW will have more profound
623 implications as they would be linked to similar trends in the interior of the
624 MedS, which have been traced back up to several decades (Rohling &
625 Bryden, 1992; Krahnmann & Schott, 1998; Bethoux, et al., 1998, Leaman &
626 Schott, 1991). Recently, Borghini et al. (2014) have concluded that the
627 MedS is becoming saltier, in which case the trend of WMDW in Table 4
628 would be nothing more than the mere reflection of this salinification.
629 Interestingly and despite being non-significant at the 95% level, a similar,
630 although proportionally reduced, salinity trend is also found in MS_{TES} at TES.

631 The intermittency of WIW is illustrated in Figure 9c. Traces of this water
632 were not found either during the INGRES cruises carried out in August and
633 November of year 2012, or during the intensive GIC survey in July the same
634 year (inset of Figure 2). It suggests that WIW was not produced this year
635 or, if yes, the volume formed was quite small. Moored-based observations
636 collected in the Gulf of Valencia near the area of WIW formation by Ribó et
637 al. (2015) identify WIW passing by the mooring line in early spring of year
638 2011, but not during late winter of year 2012. Although the authors do not
639 discard the possibility of WIW flowing above the moored instrumentation,
640 the lack of WIW, or its fainter signal, in early 2012 would be connected with
641 the absence of WIW in the SoG later on that year.

642 Almost coincidentally with this lack of WIW, the WMDW shows a relative
643 potential temperature maximum in TAC (Figure 9f) while MW_{TES} does the
644 same at TEC (Figure 8c). It would be the reflection of a rather mild 2010-11
645 winter, as discussed in Severin et al. (2014). Figure 9f shows that the
646 minimum WMDW potential temperature of all the period was reached in
647 year 2009, which could be related with an exceptional WMDW formation in
648 the Gulf of Lion (Salat, et al., 2010). There are no data available at TES this
649 year to support the observations at TAC transect, but it is noteworthy that
650 similar strong events of WMDW formation left a recognisable footprint in the
651 SoG.

652

653 Acknowledgement

654 This work is a Spanish contribution funded National Project INGRES 3
655 (CTM2010-21229), a French contribution to the "HyMeX and MOOSE
656 programmes funded by MISTRALS, and to the CIESM HYDROCHANGES
657 Programme (ciesm.org/marine/programs/hydrochanges.htm). Cristina
658 Naranjo acknowledges the fellowship BES-2011-043421 from the Ministry of
659 Economy and Competitiveness - Spain, and M. Jesús Bellanco acknowledges
660 the pre-doc fellowship BES-2011-043782. We are also grateful to the crews
661 of the R/V Angeles Alvariño and the R/V TETHYS II, and to G. Rougier (MIO)
662 and Deny Malengros (SAM/MIO) who operated the MVP. The MVP has been
663 funded through the CETSM project.

664 References

- 665 Bethoux, J., Prieur, L., & Bong, J. (1998). Warming trend in the Western
666 Mediterranean deep Water. *Nature*, 347, 660-662.
- 667 Borghini, M., Bryden, H., Schroeder, K., Sparnocchia, S., & Vetrano, A.
668 (2014). The Mediterranean is becoming saltier. *Ocean Science*, 10,
669 693-700.
- 670 Bray, N., Ochoa, J., & Kinder, T. (1995). The role of the interface in
671 exchange through the. (100), 755-776.
- 672 Bryden, H., & Stommel, H. (1982). The origin of the Mediterranean outflow.
673 40 (suppl.), 55-71. *Journal of Marine Research*, 40, 55-71.
- 674 Conan, P., & Millod, C. (1995). Variability of the northern current off
675 Marseilles, western Mediterranean Sea, from February to June 1992 .
676 *Oceanologica Acta*, 18(2), 193-205.
- 677 Criado-Aldeanueva, F., García-Lafuente, J., Vargas, J., Del Río, J., Vázquez,
678 A., Reul, A., & Sánchez, A. (2006). Distribution and circulation of
679 water masses in the Gulf of Cadiz from in situ observations. *Deep-
680 Sea REserach II*(53), 1144-1160.
- 681 Folkard, A., Davies, P., Fiúza, A., & Ambar, I. (1997). Remotely sensed sea
682 surface thermal patterns in the Gulf of Cadiz and the Strait of
683 Gibraltar: VARIability, correlations, and relationships with the surface
684 wind field. *Journal of Geophysical Research*, 102(C3), 5669-5683.
- 685 Font, J. (1987). The path of the Levantine Intermediate Water to the
686 Alboran Sea. *Dqp-Sew Research*, 24(10), 1745-1755.

- 687 Fuda, J., Millot, C., Taupier-Letage, I., Send, U., & Bocognano, J. (2000).
688 XBT monitoring of a meridian section across. *Deep-Sea Research I*,
689 47, 2191-2218.
- 690 García-Lafuente, J., Delgado, J., Sánchez-Román, A., Soto, J., Carracedo,
691 L., & Díaz del Río, G. (2009). Interannual variability of the
692 Mediterranean outflow observed. *Journal of Geophysical Research*,
693 114(C10018).
- 694 García-Lafuente, J., Sánchez-Román, A., Díaz del Río, G., Sannino, G., &
695 Sánchez-Garrido, J. C. (2007). Recent observations of seasonal
696 variability of the Mediterranean. *Journal of Geophysical Research*,
697 112(C10005).
- 698 García-Lafuente, J., Sánchez-Román, A., Naranjo, C., & Sánchez-Garrido, J.
699 (2011). The very first transformation of the Mediterranean outflow in
700 the Strait of Gibraltar. *Journal of Geophysical Research*, 116, C07010.
- 701 García-Lafuente, J., Sarhan, T., Vargas, M., Vargas, J., & Plaza, F. (1999).
702 Tidal motions and tidally induced fluxes through La Línea submarine
703 canyon, western Alboran Sea. *J. Geophys. Res.*, 104(C2), 3109-3119.
- 704 García-Lafuente, J., Vargas, J., Plaza, F., Sarhan, T., Candela, J., &
705 Bascheck, B. (2000). Tide at the eastern section of the Strait of
706 Gibraltar. *J. Geophys. Res.*, 105(C6), 14197-14213.
- 707 Gascard, J., & Richez, C. (1985). Water Masses and Circulation in the
708 Western Alboran Sea. *Progress in Oceanography*, 15, 157-216.
- 709 Hur, H., Jacobs, G., & Teague, W. (n.d.). Monthly Variations of Water
710 Masses in the Yellow and East China Seas, November 6, 1998.
711 *Journal of Oceanography*, Volume 55(2), 171-184.
- 712 Ismail, S. B., Schroeder, K., Sammari, C., & Gasparini, G. P. (2014).
713 Interannual variability of water mass properties in the. 135, 14-28.
- 714 Kim, K., Kim, K., Rhee, T., Rho, H., Limeburner, R., & Beardsley, R. (1991).
715 Identification of Water Masses in the Yellow Sea and the East China
716 Sea by Cluster Analysis. (E. O. Series, Ed.) *Oceanography of Asian
717 Marginal Seas*, 54, 253-267.
- 718 Kinder, T., & Bryden, H. (1990). Aspiration of deep waters through straits.
719 (S. Netherlands., Ed.) *In The physical oceanography of sea straits*,
720 295-319.

- 721 Kinder, T., & Parrilla, G. (1987). Yes, some of the Mediterranean outflow
722 does come from great depth. *Journal of Geophysical Research*,
723 92(C3), 2901-2906.
- 724 Krahnmann, G., & Schott, F. (1998). Longterm increases in western
725 Mediterranean salinities and temperatures: Anthropogenic and
726 climatic sources. *Geophysical Research Letters*, 25(22), 4209-4212.
- 727 Leaman, D., & Schott, F. (1991). Hydrographic structure of the convection
728 regime in the gulf of Lion: Winter 1987. *J. Phys. oceanog.*, 21, 573-
729 596.
- 730 Lopez-Jurado, J., Garcia-Lafuente, J., & Cano-Lucaya, C. (1995).
731 Hydrographic conditions of the Ibiza Channel during November 1990,
732 March 1991 and July 1992. *Oceanologica Acta*, 18(2), 235-243.
- 733 Millot, C. (1999). Circulation in the Western Mediterranean Sea. *Journal of*
734 *Marine Systems*, 20, 423-442.
- 735 Millot, C. (2009). Another description of the Mediterranean Sea outflow.
736 (82), 101-124.
- 737 Millot, C. (2013). Levantine Intermediate Water characteristics: an
738 astounding general misunderstanding! *Scientia Marina*(77(2)), 217-
739 232.
- 740 Millot, C. (2014). Heterogeneities of in- and out-flows in the Mediterranean
741 Sea. *Progress in Oceanography*(120), 254-278.
- 742 Millot, C., Candela, J., Fuda, J.-L., & Youssef, T. (2006). Large warming and
743 salinification of the Mediterranean outflow. *Deep-Sea Research I*, 53,
744 656-666.
- 745 Naranjo, C., García-Lafuente, J., Sánchez-Garrido, J., Sánchez-Román, A.,
746 & Delgado-Cabello, J. (2012). The Western Alboran Gyre helps
747 ventilate the Western Mediterranean Deep Water through Gibraltar.
748 *Deep Sea Research Part I*, 63, 157-163.
- 749 Naranjo, C., García-Lafuente, J., Sannino, G., Sánchez-Garrido, J. (2014).
750 How much do tides affect the circulation of the Mediterranean Sea?
751 From local processes in the Strait of Gibraltar to basin-scale effects.
752 *Progress in Oceanography*, 127, 108-116,
753 doi:10.1016/j.pocean.2014.06.005.

- 754 Parrilla, G., & Kinder, T. (1985). Physical oceanography of the Alboran Sea.
755 In N. A. Workshop, *Atmosphere and ocean circulation in the*
756 *Mediterranean Basin*. H. Charnock.
- 757 Parrilla, G., Kinder, T., & Preller, R. (1986). Deep and Intermediate
758 Mediterranean Water in the western Alboran Sea. *Deep-Sea*
759 *Research*, 33(1), 55-88.
- 760 Pettigrew, N. (1989). Direct measurements of the flow of western
761 Mediterranean deep water over the Gibraltar sill. *Journal of Geophys*
762 *Research*, 94(C12), 18089–18093.
- 763 Rhein, M., Send, U., Klein, B., & Krhamann, G. (1999). Interbasin deep
764 water exchange in the western. *Journal of Geophysical Research*,
765 104(C10), 23,495-23,508.
- 766 Ribó, M., Puig, P., & van Haren, H. (2015). Hydrodynamics over the Gulf of
767 Valencia continental slope and their role in sediment transport. *Deep-*
768 *Sea Research Part I*, 95, 54-66.
- 769 Rohling, E., & Bryden, H. (1992). Man-Induced Salinity and Temperature
770 Increases in Western Mediterranean Deep Water. *J. Geophys. Res.*,
771 97(C7), 11191–11198.
- 772 Salat, J., & Font, J. (1987). Water mass structure near and offshore the.
773 *Annales Geophysicae*, 5B((1)), 49-54.
- 774 Salat, J., Puig, P., & Latasa, M. (2010). Violent storms within the sea: dense
775 water formation episodes in the NW Mediterranean. *Advances in*
776 *Geosciences*, 26, 53-59.
- 777 Sánchez-Garrido, J., Sannino, G., Liberti, L., García-Lafuente, J., & Pratt, L.
778 (2011). Numerical modeling of three-dimensional stratified tidal flow.
779 *Journal of Geophysical Research*, 116(C12026).
- 780 Sánchez-Garrido, J., García-Lafuente, J., Álvarez Fanjul E., García-Sotillo,
781 M., de los Santos, F.J. (2013). What does cause the collapse of the
782 Western Alboran Gyre? Results of an operational ocean model.
- 783 Sánchez-Román, A., Criado-Aldeanueva, F., García-Lafuente, J., & Sánchez-
784 Garrido, J. (2008). Vertical structure of tidal currents over Espartel
785 and Camarinal sills,. *Journal of Marine Systems*, 74, 120-133.

- 786 Sánchez-Román, A., García-Lafuente, J., Delgado, J., Sánchez-Garrido, J., &
787 Naranjo, C. (2012). Spatial and temporal variability of tidal flow in
788 the Strait of Gibraltar. *Journal of Marine Systems*, 98-99, 9-17.
- 789 Severin, T., Conan, P., Durrieu de Madron, X., Houpert, L., Oliver, M., Oriol,
790 L., . . . Pujo-Pay, M. (2014). Impact of open-ocean convection on
791 nutrients, phytoplankton biomass and activity. *Deep Sea Research*
792 *Part I: Oceanographic Research Papers*, 94, 62-71.
- 793 Smith, R., Bryden, H., & Standsfield, K. (2008). Observations of new
794 western Mediterranean deep water formation. *Ocean Science*(4),
795 133-149.
- 796 Stommel, H., Bryden, H., & Mangelsdorf, P. (1973). Does some of the
797 Mediterranean outflow come from great depth? *Pure and Applied*
798 *Geophysics*, 105, 879-889.
- 799 Vargas-Yañez, M., Ramírez, T., Cortés, D., & Sebastián, M. (2002).
800 Warming trends in the continental shelf of Málaga Bay (Alboran Sea).
801 29(22,2082).
- 802 Vargas-Yañez, M., Zunino, P., Schroeder, K., López-Jurado, J., Plaza, F.,
803 Serra, M., Salat, J. (2012). Extreme Western Intermediate Water
804 formation in winter 2010. *Journal of Marine Systems*, 105-108, 52-
805 59.
- 806 Warn-Varnas, A., Gangopadhyay, A., Hawkins, J., & Robinson, A. (2005).
807 Wilkinson Basin area water masses: a revisit with EOFs. 25, 277-
808 296.
- 809 Weson, J., & Gregg, M. (1994). Mixing at Camarinal Sill in the Strait of
810 Gibraltar. *Journal of Geophysical Research*, 99(C5), 9847-9878.
- 811 Whitehead, J. (1985). A laboratory study of gyres and uplift near the Strait
812 of Gibraltar. *J. Geophys. Res.*, 90(C4), 7045-7060.
- 813 Yan, M. (2005). *Methods of Determining the Number of Clusters in a Data*
814 *Set and a New Clustering Criterion*. Blacksburg, Virginia: Virginia
815 Polytechnic Institute and State University.